ARMA 20–1909

SAND2020-2711C

Two-phase flow properties of a wellbore microannulus

Garcia Fernandez, S., Anwar, I., Reda Taha, M. M., Stormont, J.C.

Department of Civil Engineering, University of New Mexico, Albuquerque, NM, USA

Matteo, E.N.

Sandia National Laboratories, Albuquerque, NM, USA.

This paper was prepared for presentation at the 54th US Rock Mechanics/Geomechanics Symposium held in Golden, Colorado, USA, 28 June-1 July 2020. This paper was selected for presentation at the symposium by an ARMA Technical Program Committee based on a technical and critical review of the paper by a minimum of two technical reviewers. The material, as presented, does not necessarily reflect any position of ARMA, its officers, or members.

ABSTRACT: The interface between the steel casing and cemented annulus of a typical wellbore may de-bond and become permeable; this flow path is commonly referred to as a microannulus. Because there are often multiple fluids associated with wellbores, understanding two-phase flow behavior in the microannulus is important when evaluating the risks and hazards associated with leaky wellbores. A microannulus was created in a mock wellbore specimen by thermal debonding, which is one of the possible mechanisms for microannulus creation in the field. The specimen was saturated with silicone oil, and the intrinsic permeability through the microannulus was measured. Nitrogen was then injected at progressively increasing pressures, first to find the breakthrough pressure, and secondly, to obtain the relation between capillary pressure and gas relative permeability. The nitrogen was injected through the bottom of the specimen, to simulate the field condition where the gas migrates upwards along the casing. The measured data was successfully fit to common functional forms, such as the models of Brooks-Corey and Van Genuchten, which relate capillary pressure, saturation, and relative permeability of the two phases. The results can be used in computational models of flow along a wellbore microannulus.

1. INTRODUCTION

Wellbores provide access to the subsurface for a variety of purposes, including oil and gas production, geothermal energy, hydrocarbon and waste storage, groundwater access, and CO_2 sequestration. Leaky wellbores can compromise production or storage integrity, pollute groundwater, create hazardous operation conditions, or result in unwanted fluids at the wellhead. Among all the possible leakage paths that have been identified in the literature, the interface between the steel and cemented annulus, commonly known as a microannulus, is one of the most critical (Gasda et al., 2004). The microannulus can be formed by stresses generated by the well operation or because of cement shrinkage (Bois et al., 2011; Kjøller et al., 2016), and it has been shown that the microannulus is not expected to be uniform and it is fracture-like (Garcia Fernandez et al., 2019; Skorpa and Vrålstad, 2018; Stormont et al., 2018).

Multiple fluids, such as oil, water and gas, can be associated with wellbore operations, and thus they could be present in the microannulus, far from the common assumption where single-phases are assumed. If more than one immiscible fluid is occupying the microannulus, capillary pressures are expected to develop. Capillary pressure is the pressure between the different phases. For a fracture, it is expressed as (Pruess and Tsang, 1990):

$$P_c = \frac{2\sigma cos\theta}{a} \qquad (1)$$

where P_c is the capillary pressure between the phases (Pa), σ is the interfacial tension (N/m), θ is the contact angle between the phases (°), and a is the aperture of the fracture (m).

Relations between capillary pressures, saturation, and relative permeabilities that were originally developed for porous media such as Brooks-Corey (Brooks and Corey, 1964) or Van Genuchten (Van Genuchten, 1980) have been applied for flow through fractures because of their simplicity (Huo et al., 2014; Liu and Bodvarsson, 2001; Reitsma and Kueper, 1994; Yang et al., 2013). The Brooks-Corey model, assuming Burdine (Burdine, 1953) pore size distribution, defines the effective saturation as:

$$S_e = \frac{S-S_r}{1-S_r} = \left(\frac{P_b}{P_c}\right)^{\lambda} \; for \; P_c \geq P_b \qquad (2)$$

where S_r is the residual saturation, S is the saturation at a given capillary pressure, P_b is the bubbling pressure (breakthrough pressure), and λ is the pore-size distribution index. The relation between relative

Sandia National Laboratories is a multimission laboratory managed and operated by National Technology & Engineering Solutions of Sandia, LLC, a wholly owned subsidiary of Honeywell International Inc., for the U.S. Department of Energy's National Nuclear Security Administration under contract DE-NA0003525.

permeability and capillary pressure for both wetting and nonwetting phases is given by (assume :

$$K_{rnw} = \left[1 - \left(\frac{P_b}{P_c}\right)^{\lambda}\right]^2 \left[1 - \left(\frac{P_b}{P_c}\right)^{2+\lambda}\right] \quad (3)$$

$$K_{rw} = \left(\frac{P_b}{P_c}\right)^{2+3\lambda} \quad (4)$$

van Genuchten relates saturation, permeability, and capillary pressure:

$$K_{rw} = {S_e}^{0.5}\left[1 - \left(1 - {S_e}^{1/m}\right)^m\right]^2 \quad (5)$$

$$K_{rnw} = [1 - S_e]^{0.5}\left(1 - {S_e}^{1/m}\right)^{2m} \quad (6)$$

$$S_e = \left(\frac{1}{1+(\alpha P_c)^n}\right)^m \quad (7)$$

where α, m, and n are fitting parameters, and m and n can be often related by m = 1-1/n (Mualem, 1976).

Large scale computational models have made use of these models to investigate methane and fluid leakage from decommissioned and operative wells into the groundwater (Nowamooz et al., 2015; Rice, 2018), using parameters obtained for intact cement type G. However, wellbore leakage will undoubtedly involve flow through fractures, including the microannuli. Incorporating measured two--phase properties for microannuli will improve simulations of wellbore leakages.

2. MATERIALS AND METHODS

The specimens were comprised of a hollow steel casing surrounded by a cement sheath, simulating a wellbore configuration (Fig. 1). The thicknesses of the cement sheath and the steel casing are 30 and 2.35 mm, respectively. The outer diameter of the steel casing is 60 mm. The thickness to the inside diameter ratio used in the specimens is within the range used in oil gas wells (Gatlin, 1960).

Figure 1. Wellbore specimen used in the experiments.

Portland cement was mixed with silica fume at a weight ratio of 0.1 to provide additional strength of the cement sheath. The water/binder ratio was 0.3, and the superplasticizer was added as 2% of the water weight. The American Petroleum Institute (API) suggests using a water/binder ratio of 0.45 and no silica fume (API). Lower water/binder was used to avoid bleeding, but it is assumed that this difference would not affect the results since we are interested in the flow through the steel-cement microannulus. The cement was prepared following the ASTM (ASTM, 2014). The cement was cast around the steel casing using a PVC mold. The mold was removed after 24 h, and the specimen was placed in a water bath seven days at 65 °C.

The microannuli in the cement-steel interface was created using thermal cycles. The steel casing was filled with ice and closed on both sides using mechanical plugs. The specimen was then submerged in hot water (45 °C). The ice cools the steel, thus debonding from the cement. The hot water helps to prevent cracking induced by thermal stresses and freezing of the free water in the cement. This process was repeated several times to ensure the steel-cement debonding. Subsequent permeability measurements confirmed that a microannulus was created: the hydraulic aperture was 30 µm under 4.5MPa (650 psi) confining pressure.

2.1 Permeability measurement and gas displacement test

The experimental setup is shown in Figure 2. Endcaps were placed at the top and bottom of the sample, placing a thin perforated steel sheet in between to ensure gas distribution. A latex sleeve was holding the endcaps and the sample together and preventing any fluid loss. The specimen, endcaps, and latex sleeve were cast into a resin-based mold, thus permitting placing the specimen in a pressure vessel and performing gas and liquid testing under different confining pressures. The specimen was placed inside a pressure vessel that could apply hydrostatic stresses, and the endcaps of the sample were connected to the top endcap of the pressure vessel. The confining pressure was applied using a hydraulic pump that was connected through a port of the endcap of the pressure vessel. The specimen was oriented vertically, and the fluids were injected through the bottom of the sample and collected from the top. Gravity effects were considered in the experiment and simulate field conditions where gas migration is upwards.

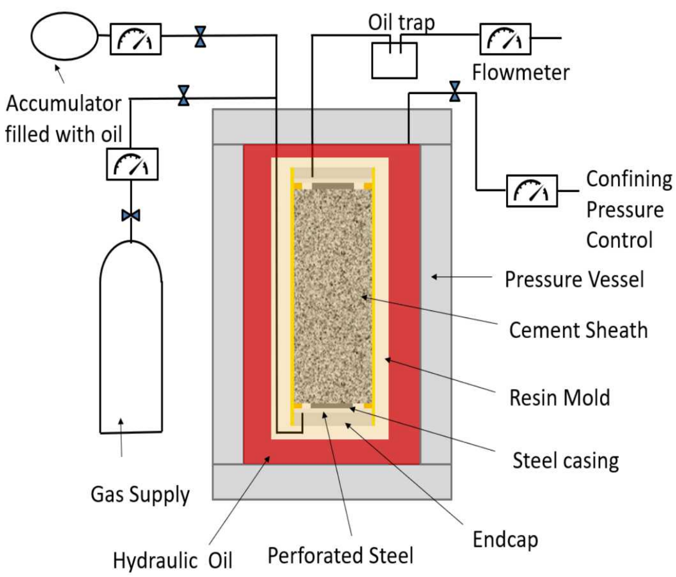

Figure 2. Schematic of the pressure vessel and the experimental setup.

The gas displacement test was performed at 4.5 MPa confining pressure. The specimen is saturated using silicone oil. Silicone oil has a viscosity of 10 Pa*s and a density of 0.935 g/cm^3. The oil was pushed through the specimen using an accumulator that was charged with nitrogen. A liquid pressure of 4 MPa (580 psi) was used to facilitate saturation. The specimen was assumed to be saturated when the liquid permeability was equal to the intrinsic permeability measured with gas. The liquid permeability was calculated using Darcy's law:

$$k = \frac{Q\mu}{\nabla PA} \qquad (8)$$

where k is the permeability (m^2), Q the volumetric flow rate (m^3/s), A the cross-sectional area involved in the flow (m^2), ∇P the pressure gradient (Pa), and μ the fluid viscosity (Pa*s). The microannulus size was estimated using the cubic law (Witherspoon et al., 1980):

$$h^3 = \frac{12Q\mu}{wi} \qquad (9)$$

where h is the hydraulic aperture (m), i is the hydraulic gradient, and w is the width of the flaw (m), which is assumed to be the outer circumference of the casing. The hydraulic aperture assumes that all the fluid flow is through the microannulus, which is consistent with experimental data (Stormont et al., 2018).

Nitrogen was pushed through the sample to displace the oil from the microannulus. Gas pressure is increased until the gas breaks through the oil and forms a continuous flow path (breakthrough pressure). Gas pressure is subsequently increased, and the flow rate measured, obtaining a dataset of gas relative permeability as a function of capillary pressure.

3. RESULTS AND DISCUSSION

3.1 Brooks-Corey and van Genuchten Parameters

The results of the gas displacement test are given in Fig. 3. The results were fitted to Brooks-Corey and van Genuchten models. The fittings parameters were calculated so that the sum of total squares between the experimental data and the model was minimized. Brooks-Corey provides a slightly better fit compared to van Genuchten (SST= 0.0043 vs SST = 0.0047)

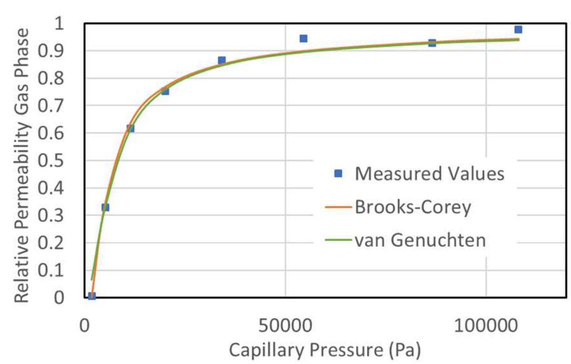

Figure 3. Experimental measurements, and fitted models of van Genuchten and Brooks-Corey.

For the Brooks-Corey Model, the bubbling pressure (measured) was 1792 Pa (0.26 psi), and λ was 0.86. van Genuchten's parameter were n = 1.80 and α = 0.02 (m^{-1}). Figures 4 and 5 show the gas and liquid relative permeabilities calculated with the fitted parameters.

Literature where the fitting parameters are provided for fractures are scarce. Yang et al., (2013) simulated a fracture with a mechanical aperture of 100 µm, changing the standard deviation of the aperture distribution, and found values of λ between 0.74 and 1.66, and breakthrough pressures ranging from 609 to 344 (Pa).

Figure 6 shows the relation between the effective saturation and the capillary pressure for both models.

The liquid permeability and saturation decrease drastically as the capillary pressure increases, so that at low capillary pressures, the saturation is very small.

The shape of the figures suggests that the microannulus is constituted by a principal channel, with larger apertures, which contributes predominantly to the total permeability, and some smaller and interconnected flow paths with smaller microannulus apertures. As the gas pressure starts to drain the microannulus, low effective saturations are reached with either model.

There is a noticeable difference between the models regarding the liquid and gas permeabilities for a given effective saturation. This difference is attributed to the different pore size distribution assumed in each model. The Brooks-Corey used here assumes Burdine (Burdine, 1953), whereas van Genuchten assumes Mualem (Mualem, 1976).

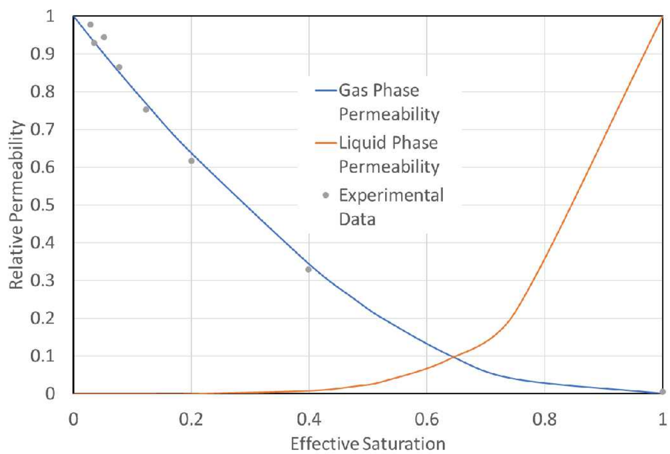

Figure 4. Brooks-Corey Model

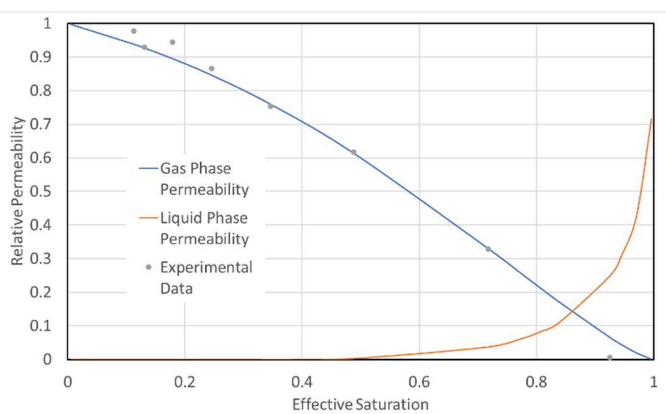

Figure 5. van Genuchten model

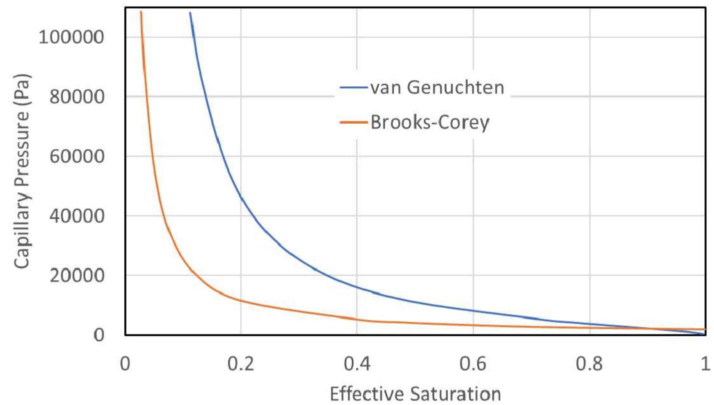

Figure 6. Effective saturation versus capillary pressure

While this study was just performed at one confining pressure, the parameters obtained in this study could be modified to account for changes in stress conditions. From tests on rock fractures, it has been shown that an increase in confining pressure will yield a decrease in the mean aperture, thus increasing the breakthrough pressure (Liu et al., 2013), it will decrease the pore size distribution index (Huo et al., 2014) and also will lower the irreducible water saturation (Huo and Benson, 2016).

3.2 Gas Breakthrough Pressure: Measured vs. Fitted

The measured gas breakthrough was 1792 Pa (0.26 psi), which indicates that with a small pressure there would be a continuous gas flow path, and the microannulus would be gas permeable.

Measuring the gas breakthrough pressure can be difficult and that there is uncertainty regarding how much time should be waited until moving to a higher pressure (Boulin et al., 2011; Hildenbrand et al., 2002). The measured breakthrough pressure was compared to the estimated pressure obtained by fitting the data assuming that the breakthrough pressure is a fitting parameter rather than an actual measurement. It was found that the fitted breakthrough pressure was 2015 Pa, which is 12% higher. The SST of the model was 0.003 vs. 0.004 obtained when using the measured breakthrough pressure.

The differences between measured and fitted breakthrough pressures are negligible. This suggests that it may not be important to try to measure the exact breakthrough pressure, thus reducing the time of the experiment.

4. CONCLUSION

We measured relative permeability and capillary pressure in a wellbore microannulus at a confining pressure of 4.5 MPa. Brooks-Corey and van Genuchten models have been successfully used to characterize two-phase flow properties of a wellbore microannulus, providing experimental data for computational models and a better understanding of its hydraulic properties.

The experimental results suggest that the microannulus was comprised of one principal channel with large apertures that controlled the hydraulic properties. The breakthrough pressure for gas migrating upwards was found at 1792Pa. In this microannulus, very small gas pressures were required to displace oil and initialize continuous gas flow.

The breakthrough pressure was both measured and fitted, and it was shown that the differences were negligible. This suggests it may not be important to measure the exact breakthrough pressure.

ACKNOWLEDGMENT

Sandia National Laboratories is a multi-mission laboratory managed and operated by National Technology and Engineering Solutions of Sandia LLC, a wholly-owned subsidiary of Honeywell International Inc. for the U.S. Department of Energy's National Nuclear Security Administration under contract DE-NA0003525. SAND2019-14056 A.

REFERENCES

API, A.P.I. (2 9). "Specification for Cements and Materials for Well Cementing." API Specification 10A: American Petroleum Institute, Washington, DC., 2009. URL

ASTM, A., 2014. 305-14 Standard practice for mechanical mixing of hydraulic cement pastes and mortars of plastic consistency ASTM C305-14. ASTM Int. West Conshohocken PA.

Bois, A.-P., Garnier, A., Rodot, F., Sain-Marc, J., Aimard, N., 2011. How to prevent loss of zonal isolation through a comprehensive analysis of microannulus formation. SPE Drill. Complet. 26, 13–31. https://doi.org/10.2118/124719-PA

Boulin, P.F., Bretonnier, P., Vassil, V., Samouillet, A., Fleury, M., Lombard, J.M., 2011. Entry pressure measurements using three unconventional experimental methods, in: International Symposium of the Society of Core Analysts. pp. 18–21.

Brooks, R., Corey, T., 1964. HYDRAU uc Properties Of Porous Media. Hydrol. Pap. Colo. State Univ. 24.

Burdine, N.T., 1953. Relative Permeability Calculations From Pore Size Distribution Data. J. Pet. Technol. 5, 71–78. https://doi.org/10.2118/225-G

Garcia Fernandez, S., Matteo, E.N., Taha, M.R., Stormont, J.C., 2019. Characterization of wellbore microannuli. J. Nat. Gas Sci. Eng. 62, 13–25. https://doi.org/10.1016/j.jngse.2018.12.003

Gasda, S.E., Bachu, S., Celia, M.A., 2004. Spatial characterization of the location of potentially leaky wells penetrating a deep saline aquifer in a mature sedimentary basin. Environ. Geol. 46, 707–720. https://doi.org/10.1007/s00254-004-1073-5

Gatlin, C., 1960. Petroleum engineering, drilling and well completions. ENGLEWOOD CLIFFS N. J. PRENTICE-HALL INC 1960 341 P.

Hildenbrand, A., Schlömer, S., Krooss, B.M., 2002. Gas breakthrough experiments on fine-grained sedimentary rocks. Geofluids 2, 3–23. https://doi.org/10.1046/j.1468-8123.2002.00031.x

Huo, D., Benson, S.M., 2016. Experimental Investigation of Stress-Dependency of Relative Permeability in Rock Fractures. Transp. Porous Media 113, 567–590. https://doi.org/10.1007/s11242-016-0713-z

Huo, D., Li, B., Benson, S.M., 2014. Investigating Aperture-Based Stress-Dependent Permeability and Capillary Pressure in Rock Fractures. Presented at the SPE Annual Technical Conference and Exhibition, Society of Petroleum Engineers. https://doi.org/10.2118/170819-MS

Kjøller, C., Torsæter, M., Lavrov, A., Frykman, P., 2016. Novel experimental/numerical approach to evaluate the permeability of cement-caprock systems. Int. J. Greenh. Gas Control 45, 86–93. https://doi.org/10.1016/j.ijggc.2015.12.017

Liu, H.-H., Bodvarsson, G.S., 2001. Constitutive relations for unsaturated flow in a fracture network. J. Hydrol. 252, 116–125. https://doi.org/10.1016/S0022-1694(01)00449-8

Liu, H.-H., Wei, M.-Y., Rutqvist, J., 2013. Normal-stress dependence of fracture hydraulic properties including two-phase flow properties. Hydrogeol. J. 21, 371–382. https://doi.org/10.1007/s10040-012-0915-6

Mualem, Y., 1976. A new model for predicting the hydraulic conductivity of unsaturated porous media. Water Resour. Res. 12, 513–522. https://doi.org/10.1029/WR012i003p00513

Nowamooz, A., Lemieux, J.-M., Molson, J., Therrien, R., 2015. Numerical investigation of methane and formation fluid leakage along the casing of a decommissioned shale gas well. Water Resour. Res. 51, 4592–4622. https://doi.org/10.1002/2014WR016146

Pruess, K., Tsang, Y.W., 1990. On two-phase relative permeability and capillary pressure of rough-walled rock fractures. Water Resour. Res. 26, 1915–1926. https://doi.org/10.1029/WR026i009p01915

Reitsma, S., Kueper, B.H., 1994. Laboratory measurement of capillary pressure-saturation relationships in a rock fracture. Water Resour. Res. 30, 865–878. https://doi.org/10.1029/93WR03451

Rice, A.K., 2018. Groundwater-quality implications of methane leakage from hydrocarbon wellbores (Thesis). Colorado School of Mines. Arthur Lakes Library.

Skorpa, R., Vrålstad, T., 2018. Visualization of Fluid Flow Through Cracks and Microannuli in Cement Sheaths. SPE J. https://doi.org/10.2118/180019-PA

Stormont, J.C., Garcia Fernandez, S., Taha, M.R., Matteo, E.N., 2018. Gas flow through cement-casing microannuli under varying stress conditions.

Geomech. Energy Environ. 13, 1–13. https://doi.org/10.1016/j.gete.2017.12.001

Van Genuchten, M.Th., 1980. A Closed-form Equation for Predicting the Hydraulic Conductivity of Unsaturated Soils 1. Soil Sci. Soc. Am. J. 44, 892–898. https://doi.org/10.2136/sssaj1980.03615995004400050002x

Witherspoon, P.A., Wang, J.S.Y., Iwai, K., Gale, J.E., 1980. Validity of Cubic Law for fluid flow in a deformable rock fracture. Water Resour. Res. 16, 1016–1024. https://doi.org/10.1029/WR016i006p01016

Yang, Z., Niemi, A., Fagerlund, F., Illangasekare, T., 2013. Two-phase flow in rough-walled fractures: Comparison of continuum and invasion-percolation models. Water Resour. Res. 49, 993–1002. https://doi.org/10.1002/wrcr.20111